TABLE 4. BONE MINERAL DENSITY AT RABBIT SKULL DEFECTS IN 8 WEEKS AFTER APPLICATION

Application	*Hydrogel water content (wt%)*	*BMD (mg/cm^2)*
PBS		45.9 ± 10.7*
Free BMP-2		65.4 ± 10.5
Empty gelatin hydrogel	97.8	38.0 ± 3.2*
Gelatin hydrogel incorporating BMP-2	93.8	57.4 ± 11.5*
	97.8	87.3 ± 6.4
	99.7	62.7 ± 8.0*
IBM		58.3 ± 13.3*

The BMP-2 dose was 5 μg/site.

The BMD of intact rabbit skulls was 122.9 ± 12.1 mg/cm^2.

*$p < 0.05$, significant against the BMD value at the skull bone defect after application of gelatin hydrogels incorporating BMP-2 with a water content of 97.8 wt%

the IBM that incorporated BMP-2. The BMP-2 dose was 5 μg/site. As was seen with the monkey model, the BMD at the skull defect to which gelatin hydrogel with a water content of 97.8 wt% had been applied was significantly increased. Other applications did not increase the BMD.

DISCUSSION

The present study demonstrates that at the site of defects in the skulls of nonhuman primates (monkeys), bone regeneration induced by gelatin hydrogels that incorporated BMP-2 was greatly influenced by the water content of hydrogels and BMP-2 doses. In general, when osteogenic BMP-2 is applied to the bone defect in a large animal model, bone regeneration requires higher doses than those needed for rodents.[16,17] The difference in dose among the animal species is attributed to the number of responding cells, the rates of fracture healing, and the retention time of osteogenic growth factors. If carrier systems for the sustained release of osteogenic growth factors are developed, not only efficient bone formation but also decrease in the dose are expected. We explored carrier systems composed of gelatin hydrogels with different water contents. The water content could be easily changed only by altering the concentration of gelatin and glutaraldehyde in a crosslinking reaction (Table 1). A previous study showed that the water content of hydrogels successfully regulated the *in vivo* controlled-release profile of BMP-2.[10] The release period of BMP-2 became longer with a decrease in the water content of the hydrogels. The profile of BMP-2 release was in good accordance with that of hydrogel degradation, indicating that BMP-2 release is governed by the degradation of the hydrogel carriers. Furthermore, we have experimentally demonstrated that significantly higher bone formation was induced by the BMP-2–incorporated gelatin hydrogel with a water content of 97.8 wt% than with the lower or higher water contents, both in the muscle of rats and the ulna defect of rabbits.[10,11] These findings indicate that the release period of BMP-2 may be essential to promoting bone induction activity.

For this study, we selected a 6-mm-diameter skull defect in monkeys. Radiographic and histologic observations revealed no bone regeneration for the control defect applied with PBS and the empty gelatin hydrogel (Fig. 1A and E or Fig. 2A and E). This indicates that the hydrogel itself had no ability to induce bone regeneration. The bone regeneration at the defect applied with BMP-2 solution was also similar to that at defects to which PBS was applied and the empty gelatin hydrogel, even if the dose of BMP-2 in the free BMP-2 solution was 200 μg (Table 3 and Fig. 3). These results strongly indicate that the size of defect used to assess bone regeneration should be large enough to prevent spontaneous healing. The application of materials without any osteoinduction activity into the skull bone defect results in the formation of fibrous connective tissue rather than bone (Fig. 1A and E).

The ability of gelatin hydrogels that incorporated BMP-2 to induce bone regeneration greatly depended on their water content (Tables 3 and 4 and Figs. 1 and 2). It is likely that the fast-degraded hydrogel could neither prolong the *in vivo* retention of BMP-2 nor protect the defect from the ingrowth of fibrous tissue. When the rate of hydrogel degradation is too slow compared with that of bone regeneration at the skull defect, it is likely that the hydrogel remaining in the defect physically impairs bone regeneration, even though BMP-2 is released over the long term. Our previous studies experimentally confirmed that gelatin hydrogels with a slow degradability physically impaired bone regeneration induced by gelatin hydrogels that incorporated osteogenic growth factor at both the ulna and skull defect models of rabbits.[10,11] The osteoinduction activity of the hydrogel with a water content of 97.8 wt% was significantly higher than that of the hydrogel with higher and lower water content.[10] Interestingly, the present dependency of the osteoinduction activity for gelatin hydrogels that incorporated BMP-2 is highly correlated to that observed in the previous study. These findings indicate that a balance in the profile between BMP-2 retention and bone formation is essential for the bone regeneration induced by gelatin hydrogels that incorporate BMP-2.

In clinical application, a collagen sponge (reconstituted from bovine tendon) and collagen-based matrix (derived from IBM) have been used as the material for the sustained release of BMPs. A series of preclinical studies suggest that the carriers pharmacologically allowed the proteins to stimulate the activity of local bone induction.[18,19] IBM is one of the materials to be investigated as a promising carrier for reducing the BMP-2 dose.[12,13] This study also confirmed that IBM enhanced bone regeneration at the skull defects (Figs. 1 and 2). However, the BMD was significantly lower than that of the gelatin hydrogel that was able to provide 4-week

release of BMP-2. Although several factors may explain the increased BMD, the time period of BMP-2 release may be one of major contributors to the gelatin superiority. Indeed, the time period of BMP-2 was different between gelatin hydrogel and IBM, as shown in previous study.[12] On the other hand, our previous study indicated that the collagen sponge that incorporated BMP-2, which released BMP-2 for 2 weeks, showed enhanced osteoinduction activity at the subcutaneous tissue around the implanted site but exhibited lower osteoinduction activity than the gelatin hydrogel.[10] Therefore, optimization of the release profile of BMP-2 by the scaffold design may be important to promote bone regeneration and reduce the BMP-2 dose.

Many clinical trials have used BMP-incorporated scaffolds for indications such as treatment of fractures, enhancement of spinal fusion, and reconstruction of areas with large bone loss.[20–25] The osteogenetic products composed of BMP-7 (osteogenic protein-1) and collagen are commercially available.[26] However, high doses of BMPs are generally required for those applications. Indeed, the BMP concentration of the commercially available product was 3.5 mg/g,[26] and bone regeneration in the clinical trials requires at least more than 1 mg/mL of BMP.[20–25] High doses of BMPs can promote bone regeneration but eventually will cause systemic side effects.[2,27,28] In this study, bone regeneration at monkey skull defects was significantly enhanced even at a BMP-2 dose of 5 μg/site, a dose as low as that used in rabbits (Tables 3 and 4). This BMP-2 dose is extremely low compared with that used for other materials that have been clinically studied. To reduce the physical and psychological burdens of patients, shortening the period required for bone regeneration is necessary. Generally, bone repair is not complete until more than 6 months after surgery.[29] With the gelatin hydrogel that incorporates BMP-2, the BMD was recovered at the same level of the intact skulls 12 weeks after surgery; this was a much shorter period than that seen with the IBM that incorporated BMP-2 (Fig. 3). This difference between the hydrogel system and the gold standard IBM may be attributed to biological harmonization of BMP-2 release and material degradation. With the hydrogel system, biologically active BMP-2 is retained at the defect for an optimal time period, while the hydrogel release carrier degrades until it disappears from the defect, leaving no physical impairment for the physiologic process of bone regeneration. However, this situation is not always expected for IBM or other materials.

In conclusion, through the controlled-release technology provided by the gelatin hydrogel for an appropriate time period, a low dose of BMP-2 induced osteoinduction for nonhuman primates.

ACKNOWLEDGMENT

We thank Professor Emeritus Yoshinori Kuboki, Department of Oral Health Science, Graduate School of Dental Medicine, Hokkaido University, Hokkaido, Japan, for supplying IBM.

REFERENCES

1. Wozney, J.M., and Rosen, V. Bone morphogenetic protein and bone morphogenetic protein gene family in bone formation and repair. Clin. Orthop. Relat. Res. **346,** 26, 1998.
2. Hollinger, J.O., Uludag, H., and Winn, S.R. Sustained release emphasizing recombinant human bone morphogenetic protein-2. Adv. Drug. Deliv. Rev. **31,** 303, 1998.
3. Uludag, H., D'Augusta, D., Palmer, R., Timony, G., and Wozney, J. Characterization of rhBMP-2 pharmacokinetics implanted with biomaterial carriers in the rat ectopic model. J. Biomed. Mater. Res. **46,** 193, 1999.
4. Boyne, P.J., Marx, R.E., Nevins, M., Triplett, G., Lazaro, E., Lilly, L.C., Alder, M., and Nummikoski, P. A feasibility study evaluating rhBMP-2/absorbable collagen sponge for maxillary sinus floor augmentation. Int. J. Periodont. Rest. Dent. **17,** 11, 1997.
5. Geiger, M., Li, R.H., and Friess, W. Collagen sponges for bone regeneration with rhBMP-2. Adv. Drug. Deliv. Rev. **55,** 1613, 2003.
6. Hollinger, J.O., Schmitt, J.M., Buck, D.C., Shannon, R., Joh. S.P., Zegzula, H.D., and Wozney, J. Recombinant human bone morphogenetic protein-2 and collagen for bone regeneration. J. Biomed. Mater. Res. (Appl. Biomater.) **43,** 356, 1998.
7. Urist, M.R., Lietze, A., and Dawson, E. β-tricalcium phosphate delivery system for bone morphogenetic protein. Clin. Orthop. Relat. Res. **187,** 277, 1984.
8. Zegzula, H.D., Buck, D.C., Brekke, J., Wozney, J.M., and Hollinger, J.O. Bone formation with use of rhBMP-2 (recombinant human bone morphogenetic protein-2). J. Bone Joint Surg. Am. **79,** 1778, 1997.
9. Wheeler, D.L., Chamberland, D.L., Schmitt, J.M., Buck, D.C., Brekke, J.H., Hollinger, J.O., Joh, S.P., and Suh, K.W. Radiomorphometry and biomechanical assessment of recombinant human bone morphogenetic protein-2 and polymer in rabbit radius osteotomy model. J. Biomed. Mater. Res. (Appl. Biomater.) **43,** 365, 1998.
10. Yamamoto, M., Takahashi, Y., and Tabata, Y. Controlled release by biodegradable hydrogels enhances the ectopic bone formation of bone morphogenetic protein. Biomaterials **24,** 4375, 2003.
11. Yamamoto, M., Takahashi, Y., and Tabata, Y. Enhanced bone regeneration at a segmental bone defect by controlled release of bone morphogenetic protein-2 from a biodegradable hydrogel. Tissue Eng. **12,** 1305, 2006.
12. Takita, H., Vehof, J.W., Jansen, J.A., Yamamoto, M., Tabata, Y., Tamura, M., and Kuboki, Y. Carrier dependent cell differentiation of bone morphogenetic protein-2 induced osteogenesis and chondrogenesis during the early implantation stage in rats. J. Biomed. Mater. Res., **71A,** 181, 2004.
13. Vehof, J.W., Takita, H., Kuboki, Y., Spauwen, P.H., and Jansen, J.A. Histological characterization of the early stages of bone morphogenetic protein-induced osteogenesis. J. Biomed. Mater. Res. **71,** 181, 2004.
14. Tabata, Y., Yamada, K., Liu, H., Miyamoto, S., Hashimoto, N., and Ikada, Y. Skull bone regeneration in primates in response to basic fibroblast growth factor. J. Neurosurg. **91,** 851, 1999.

15. Yamada, K., Tabata, Y., Yamamoto, K., Miyamoto, S., Nagata, I., Kikuchi, H., and Ikada, Y.J. Potential efficacy of basic fibroblast growth factor incorporated in biodegradable hydrogels for skull bone regeneration. Neurosurgery **86,** 871, 1997.
16. Yoon, S.T., and Boden, S.D. Osteoinductive molecules in orthopaedics: basic science and preclinical studies. Clin. Orthop. Relat. Res. **395,** 33, 2002.
17. Seeherman, H., Li R., and Wozney, J. A review of preclinical program development for evaluating injectable carriers for osteogenic factors. J. Bone Joint Surg. **Suppl. 3,** 96, 2003.
18. Friess, W., Uludag, H., Foskett, S., Biron, R., and Sargeant, C. Characterization of absorbable collagen sponges as rhBMP-2 carriers. Int. J. Pharm. **187,** 91, 1999.
19. Uludag, H., D'Augusta, D., Golden, J., Li, J., Timony, G., Riedel, R., and Wozney, J.M. Implantation of recombinant human bone morphogenetic proteins with biomaterial carriers; a correlation between protein pharmacokinetics and osteoinduction in the rat ectopic model. J. Biomed. Mater. Res. **50,** 227, 2000.
20. Cook, S.D., Baffes, G.C., Wolfe, M.W., Sampath, T.K., and Rueger, D.C. The effect of recombinant human osteogenetic protein-1 on healing of large segmental bone defects. J. Bone Joint Surg. **76,** 827, 1994.
21. Groeneveld, E.H., van den Bergh, J.P., Holzmann, P., ten Bruggenkate, C.M., Tuinzing, D.B., and Burger, E.H. Histomorphometrical analysis of bone formed in human maxillary sinus floor elevations grafted with OP-1 device, demineralized bone matrix or autogenous bone. Comparison with non-grafted sites in a series of case reports. Clin. Oral. Implants Res. **10,** 499, 1999.
22. Geesink, R.G., Hoefnagels, N.H., and Bulstra, S.K. Osteogenetic activity of OP-1 bone morphogenetic protein (BMP-7) in a human fibular defect. J. Bone Joint Surg. **81,** 710, 1999.
23. Boden, S.D., Zdeblick, T.A., Sandhu, H.S., and Heim, S.E. The use of rhBMP-2 in interbody fusion cages. Definitive evidence of osteoinduction in humans: a preliminary report. Spine **25,** 376, 2000.
24. Friedlaender, G.E., Perry, C.R., Cole, J.D., Cierny, G., Muschler, G.F., Zych, G.A., LaForte, A.J., and Yin, S. Osteogenic protein-1 (bone morphogenetic protein-7) in the tibial nonunions. J. Bone Joint Surg. Am. **83-A Suppl 1,** S151, 2001.
25. Einhorn, T.A. Clinical applications of recombinant human BMPs: early experience and future development. J. Bone Joint Surg. Am. **85-A Suppl 3,** 82, 2003.
26. Mont, M.A., Ragland, P.S., Biggins, B., Friedlaender, G., Ptel, T., Cook, S., Etienne, G., Shimmin, S., Kildey, R., Rudger, D.C., and Einhorn, T.A. Use of bone morphogenetic proteins for musculoskeletal applications. An overview. J. Bone Joint Surg. Am. **86-A Suppl 2,** 41, 2004.
27. Gittens, S.A., and Uludag, H. Growth factor delivery for bone tissue engineering. J. Drug Targ. **9,** 407, 2001.
28. Lieberman, J.R., Daluiski, A., and Einhorn, T.A. The role of growth factors in the repair of bone. Biology and clinical applications. J. Bone Joint Surg. Am. **84-A,** 1032, 2002.
29. Valentin-Opran, A., Wozney, J., Csimma, C., Lilly, L., and Riedel, G.E. Clinical evaluation of recombinant human bone morphogenetic protein-2. Clin. Orthop. Relat. Res. **395,** 110, 2002.

Address reprint requests to:
Yasuhiko Tabata, Ph.D.
Institute for Frontier Medical Sciences
Kyoto University
53 Kawara-cho Shogoin
Sakyo-ku Kyoto 606-8507
Japan

E-mail: yasuhiko@frontier.kyoto-u.ac.jp

Journal of
Nanoscience and Nanotechnology
Vol. 7, 763–772, 2007

RESEARCH ARTICLE

Effect of Pore Size of Self-Organized Honeycomb-Patterned Polymer Films on Spreading, Focal Adhesion, Proliferation, and Function of Endothelial Cells

Masaru Tanaka[1, 2, *, †], Aiko Takayama[2], Emiko Ito[2], Hiroshi Sunami[1, 2], Sadaaki Yamamoto[1, 2], and Masatsugu Shimomura[2, 3]

[1] *Creative Research Initiative "Sousei", Hokkaido University, Kita-Ku N21W10, Sapporo 001-0021, Japan*
[2] *CREST, Japan Science and Technology Corporation, Honchou 4-1-8, Kawaguchi 332-0012, Japan*
[3] *Nanotechnology Research Center, Research Institute for Electronic Science, Hokkaido University, Kita-Ku N21W10, Sapporo 001-0021, Japan*

The design of nano- and microstructures based on self-organization is a key area of research in the search for new materials, and it has a variety of potential applications in tissue engineering scaffolds. We have reported a honeycomb-patterned polymer film (honeycomb film) with highly regular pores that is formed by self-organization. This study describes the behavior of vascular endothelial cells (ECs) on honeycomb films with four different pore sizes (5, 9, 12, and 16 μm) as well as on a flat film. We examined the influence of the honeycomb pattern and pore size on cell behavior. The changes in cell morphologies, actin filaments, vinculin clusters, cell proliferation, and secreted extracellular matrix (ECM) (fibronectin, laminin, type IV collagen, and elastin) production profiles were observed by using optical, fluorescence, and scanning electron microscopy. The ECs that adhered to the flat film showed an elongated morphology with random orientation; the actin filaments and focal adhesions were not conspicuous. On the other hand, the ECs on the honeycomb films exhibited greater spreading and flattening; the degree of spreading of the ECs increased with an increase in the pore size. The actin filaments and focal adhesions appeared conspicuous, and the focal adhesions localized along the edge of the honeycomb pores were distributed over the entire projected cell area. The honeycomb film with a pore size of 5 μm showed the highest cell proliferation and ECM production profiles. These results suggest that the honeycomb film is a suitable material for designing a new vascular device.

Keywords: Cell Adhesion, Self-Organization, Scaffold, Pore Size, Focal Adhesion.

1. INTRODUCTION

Porous scaffolds fabricated from biodegradable polymers have been widely used as temporary extracellular matrices (ECMs) and play critical roles in tissue engineering and *in situ* tissue reconstruction.[1–4] Scaffolds with appropriate porosities and interconnected pores are required to facilitate cell adhesion, ECM secretion, and eventual tissue regeneration. A number of fabrication methods, including phase separation and lithography techniques, have been developed and applied to the fabrication of porous scaffolds from biodegradable polymers.[5–11] These techniques are certainly useful in the fabrication of porous scaffolds. However, these techniques require a large amount of energy and involve many processes. In addition, a limited variety of materials is available for scaffolds. Each of these approaches is very different and has a unique set of characteristics that have some limitations, including uncontrolled pore size and size distribution. As a result, there is a high demand for suitable alternative methods for preparing scaffolds. Inspired by biology, the self-organization of organic and inorganic components into hierarchical and sophisticated structures offers an alternative to the conventional techniques of nano- and microfabrication. The process occurs under ambient physiological conditions in contrast to typical fabrication techniques that

*Author to whom correspondence should be addressed.
†Present address: Nanotechnology Research Center, Research Institute for Electronic Science, Hokkaido University, Kita-Ku N21W10, Sapporo 001-0021, Japan

1533-4880/2007/7/763/010 doi:10.1166/jnn.2007.514

require harsh conditions. It can be applied to polymer fabrication because of its physical generality. We have found that typical regular structures are formed during the process of casting of polymer solutions on solid surfaces; for example, self-organized honeycomb-patterned polymer films (honeycomb films) with highly regular porous structures can be prepared under humid casting conditions.[12–24] The pore size can be controlled in the range of 100 nm to 50 μm by changing the casting conditions. This method has a great advantage in that the films can be prepared with ease, at a low cost, and without any limitations pertaining to the availability of materials for the scaffold. The process is relatively easy to scale up and is being used for the commercial production of porous scaffolds.

The impact of the surface topography of a polymer on cell adhesion was a matter of concern because the nano- and microscale pattern of a surface can exert a significant effect on the adhesion behavior of cells on the surface.[25–27] In particular, the pore size of a tissue engineering scaffold could influence cell adhesion and subsequently, their proliferation. One of the keys in vascular tissue engineering and bioartificial vessel development is the design of a porous polymer scaffold of effective pore size for facilitating the adhesion and functions of vascular endothelial cells (ECs).[28] However, it is difficult to control the adhesion of these cells and enhance their functions *in vitro*. Additionally, EC activities are often limited by the lack of an EC-specific environment.

Here, we describe the fabrication of honeycomb films by using a solution casting technique under humid air conditions. Additionally, we also examined a culture of ECs on these films in order to investigate the influence of the honeycomb pattern and the pore size on cell morphologies, actin filaments, vinculin clusters, proliferation, and secreted ECM (fibronectin, laminin, type IV collagen, and elastin) production profiles. These regular arrays of pores allowed the specific interactions of the cells. The influence of pore size on cell adhesion and proliferation or function may provide valuable information for designing appropriate polymer scaffolds used in vascular tissue engineering.

2. EXPERIMENTAL DETAILS

2.1. Materials

Honeycomb films were fabricated using biodegradable polymers poly(ε-caprolactone) (PCL; MW = 70,000–100,000; Fig. 1(a)) and a copolymer of dodecylacrylamide and ω-carboxyhexylacrylamide (Cap; MW = 22,000; Fig. 1(b)). Cap was used as an emulsifier in this study. The copolymer was synthesized by using a previously reported method.[29] The copolymer is amphiphilic because the polymer forms a stable monolayer at the air–water interface. The water was purified by a Millipore system (Milli-Q, Millipore). Organic solvents and other

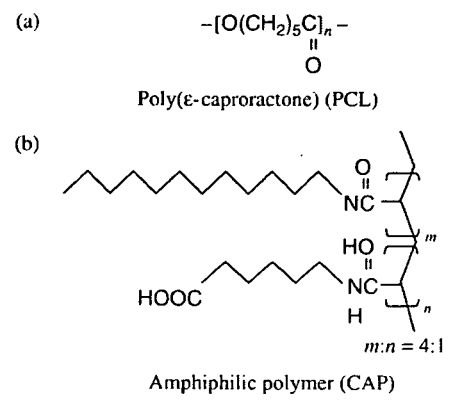

Fig. 1. Chemical structures of (a) poly(ε-caprolactone) (PCL) and (b) copolymer of dodecylacrylamide and ω-carboxyhexylacrylamide (Cap).

chemicals were commercially available and were used without further purification.

2.2. Preparation of Honeycomb and Flat Films

The honeycomb film was prepared on a glass substrate by employing a previously described method.[15–23] In brief, PCL and Cap (10:1 wt%) were dissolved in chloroform at a concentration of 5 g/L. The polymer solution was poured into a round glass dish (9.3 cm in diameter) with blowing of highly humid air (1.0 L/min). The flat film was prepared as follows. The PCL and Cap solution (5 g/L) was poured onto a glass slide. The cover glass with the polymer layer was spun at 1000 rpm for 30 s using a spin coater (1H-7D, Mikasa). These films were immersed in 1-propanol for 12 min to remove Cap. The static contact angle of the films was measured at room temperature (23 °C–25 °C) by sessile drop method using a contact angle goniometer (Face CA-A, Kyowa Interface Science).

2.3. Culturing of ECs

Porcine aortic ECs (CSC Certificate™ Dainippon Pharmaceutical) were purchased. The frozen cells were thawed at 37 °C and then resuspended in a culture medium (Dulbecco's Modified Eagle's Minimal Essential Medium, Sigma). Subsequently, 10% fetal bovine serum (FBS), 100 unit/ml penicillin, and 100 μg/ml penicillin-streptomycin (Gibco) were added. A honeycomb film and a flat film on a glass plate were preincubated in a culture medium for 72 h at 37 °C in 5% CO_2 before cell seeding. The ECs were seeded on the films at a density of 1.5×10^4 cells/cm^2. The ECs at passages 6–8 were used in the experiments. In preliminary experiments, we established that the differences in passage number did not affect the outcome of our study. The culture medium was replaced after days 1, 3, 5, and 7 without damaging the films. The morphologies of the ECs after seeding were observed under a phase contrast microscope (IX 70, Olympus) until the ECs proliferated to confluence. After 1 to 9 days of

RESEARCH ARTICLE

culture, the number of ECs on each film was evaluated with the cell proliferation reagent WST-1 (F. Hoffmann-La Roche).

2.4. Scanning Electron Microscopic Observation

The ECs that were cultured 1 to 9 days after seeding were fixed in 2% glutaraldehyde in phosphate-buffered saline (PBS; Wako) and were incubated over night at 4 °C. After washing three times with PBS, each sample was fixed in 1.0% osmium tetroxide (Wako) aqueous solution for 1 h and was rinsed in PBS. Subsequently, the samples were dehydrated by washing in increasing concentrations of ethanol and were then air dried. The samples were transferred to microporous specimen capsules and dried by means of a critical point dryer (HCP-2, Hitachi). The dried samples were mounted on aluminum stages by using double-stick tape, and they were coated with palladium gold (approximately 5 nm of coating) by using an ion sputter coater (E-1030, Hitachi). All samples were observed using a scanning electron microscope (SEM; S-3500N, Hitachi).

2.5. Actin, Vinculin, and ECM Staining by Confocal Laser Scanning Microscopy

The actin filaments in the ECs that were cultured 5 days after seeding were stained. After washing with PBS, the cells were fixed with 10% formaldehyde (Wako) for 30 min at 22 °C. The cells were washed twice with PBS and permeated with 1% Triton X-100 in PBS solution for 5 min at 22 °C and 1.0% bovine serum albumin (Sigma) in PBS. To visualize the cytoskeletal element actin fiber, focal adhesion vinculin, and ECM (fibronectin, laminin, type IV collagen, and elastin) production profiles, staining was performed by an immunological method using primary antibodies (diluted 1:100, Chemicon) for each antigen and fluorescence-labeled secondary antibodies (diluted 1:1000; Alexa Fluor 546 goat anti-mouse IgG or Alexa Fluor 488 phalloidin, Molecular Probes). The stained cells were rinsed four times with PBS, and subsequently immersed for 1 h at the fourth rinse. All samples were applied to slides. Coverslips were placed on the samples and sealed with nail polish. A confocal laser scanning microscope (CLSM; FV-300, Olympus) was used for observation. The projected areas and the number of focal adhesions of isolated cells on the film were analyzed with an NIH image software.

3. RESULTS AND DISCUSSION

3.1. Honeycomb Film

The SEM showed a highly regular hexagonal arrangement of pores (honeycomb-patterned structure), and a well

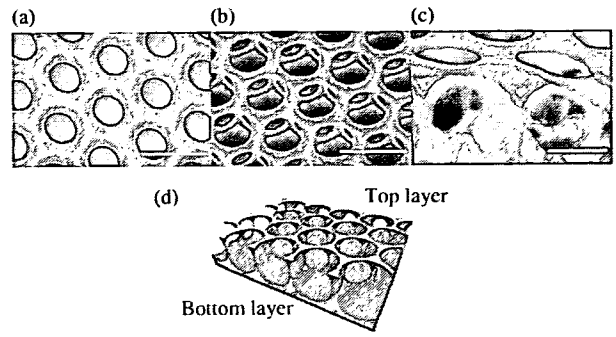

Fig. 2. SEM images of the honeycomb film (a) surface, (b) tilted, and (c) cross section. (d) Schematic representation of the 3-D structure of the honeycomb film. The pore structure (spherical shape) reflects the use of water droplet as a template.

interconnected, uniform pore structure (pore size: approximately 5 μm; Figs. 2(a–c)). The 3-D structure could affect the flow of nutrients and wastes. A schematic cross section of this regular microporous film is shown in Figure 2(d). Condensation due to the evaporation cooling of humid air occurred when a water-immiscible solvent was used. Self-packed and mono-dispersed water droplets that formed on the solution surface act as a temporary template for pores. In general, the condensed water droplets are not stable and eventually start coalescing. In order to prepare a highly regular porous (honeycomb-patterned) film, the stabilization of the water droplets is necessary. The role of the amphiphilic polymer in pattern formation is to prevent the fusion of the water droplets. Cap (Fig. 1(a)) acts as a surfactant and contributes to the stabilization of the water droplets at the interface of the polymer solution and water. As a result, the fusion of the water droplets is prevented due to the intervening amphiphilic polymer layer. Most polymers dissolved in a water-immiscible solvent can be fabricated to a honeycomb film by the addition of Cap. Various experimental factors affected the pore structures. A uniform pore size can be achieved by changing the casting conditions.[12–23] In this study, honeycomb films with four different pore sizes, 5, 9, 12, and 16 μm, that were narrower than the diameter of an EC in suspension were prepared by changing the casting volume (Fig. 3 and Table I). The rim of the honeycomb films widened with an increase in the pore size. The length of pore edge per unit surface area is greatest in the smaller pore size. The porosity of each film was approximately 50%. The contact angles of the honeycomb films were approximately 105° regardless the pore size. This indicates an increase in the hydrophilicity when compared with a flat film with a contact angle of 74°. Unlike other template or lithographic methods, the advantage of this method is the ease with which patterned surfaces can be fabricated using various materials without the consumption of a large amount of energy. In this study, PCL was selected as the matrix polymer due to its highly pliable nature.

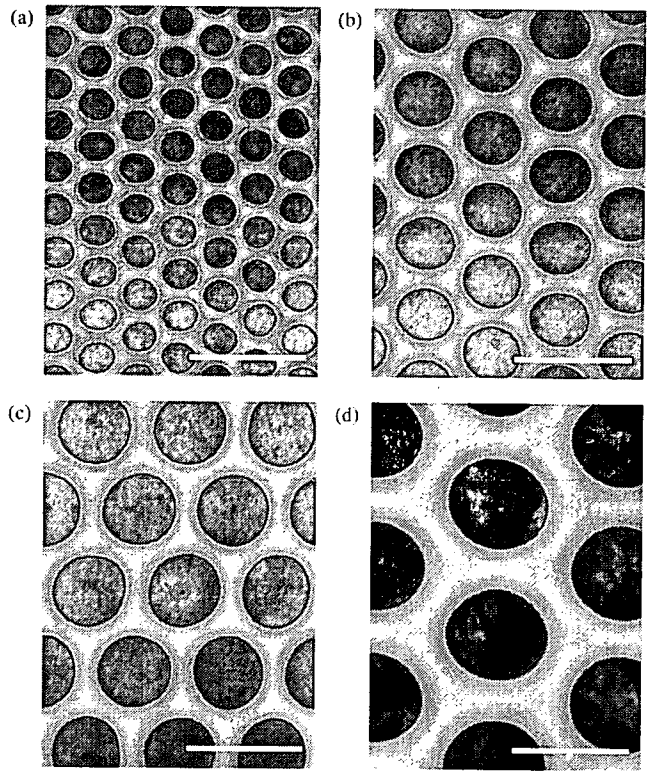

Fig. 3. SEM images of the honeycomb films. The pore sizes were approximately (a) 5 μm, (b) 9 μm, (c) 12 μm, and (d) 16 μm. Bar: 20 μm.

3.2. Morphologies of Adhered ECs on Honeycomb and Flat Films

Most tissue-derived cells are anchorage dependent and require attachment to a solid surface for viability and growth. For this reason, the initial events that occur when a cell approaches a surface are of fundamental interest. In tissue engineering, cell adhesion to a surface is critical because adhesion precedes other events, such as cell spreading, cell migration, and differentiated cell functions. The ability of the honeycomb film to support an EC culture was investigated *in vitro*. The adhesion and proliferation behavior of the ECs and their morphology on the honeycomb films were characterized on the basis of SEM observation. Figure 4 shows the morphology of ECs adhering on the films after 5 days of incubation. The morphology of the ECs on the honeycomb film was compared with that of those on the flat film. Different EC morphologies were observed on both the films. The ECs on the flat film showed an elongated morphology with random orientation (Figs. 4(a, d)). The flat film restricted cell spreading but did not inhibit cell adhesion. The ECs attached to the honeycomb films exhibited greater cell spreading and flattening. Small protrusions were observed around the ECs. The ECs were well spread along the honeycomb rims; this was maintained at least until the cells reached near confluence. This behavior is expected to exhibit better and prolonged EC function. Several parameters have been used to describe cell shape and spreading.[30] For comparison, the cell projected area was used to quantify the morphological response of cells that showed spreading on the films. The average EC projected area on the flat film was approximately 2,500 μm^2 and that on the honeycomb films was approximately 4,200 μm.[2] These results showed that greater cell adhesion could be achieved on a honeycomb film compared to a flat film. The honeycomb film has an adhesive property since the monolayer was appeared on the surface with the adhesive property. The cells could adhere and spread along the honeycomb pattern, but they did not extend into the pores of the honeycomb film via cell protrusions. Significant differences in the cell shape were found depending on the pore size of the honeycomb films. The degree of spreading of the ECs was enhanced with an increase in the pore size. It was observed that the thickness of the cells on the honeycomb film with 5 μm pores (Figs. 4(b, e)) was higher than that of those on the honeycomb film with 16 μm pores (Figs. 4(c, f)). This showed that the cells prefer to spread on a honeycomb film with a large pore size. It should be noted that both the flat and honeycomb films were prepared from the same polymer. This implies that the topological property of the honeycomb film affected the EC morphology. The honeycomb film may be appropriate for regulating the degree of cell–cell and cell–material interactions. The honeycomb pattern variations may also affect EC-specific functions. Further investigation is required for elucidating the mechanism of the interaction between ECs and the honeycomb film. However, the strategy of immobilization and stabilization of ECs through the use of honeycomb films would prove advantageous in designing a bioartificial vascular device, wherein the ECs could attach to a film with a high surface area, maintain their functions, and remain stable against the perfusion and shear forces in the blood vessel.

Table I. Properties of honeycomb and flat films.

	Flat film	Honeycomb films			
Pore size (μm)	—	5.3 (±0.02)	9.1 (±0.03)	11.8 (±0.15)	15.6 (±0.08)
Rim size (μm)	—	1.8 (±0.06)	3.1 (±0.20)	3.6 (±0.35)	7.1 (±0.15)
Poro edge length (μm)*	—	258.7 (±2.32)	187.9 (±2.81)	162.0 (±4.15)	87.3 (±2.73)
Porosity (%)	—	50.6 (±0.73)	51.0 (±1.65)	54.7 (±3.60)	42.6 (±13.63)
Contact angle (°)	73.9 (±1.45)	105.6 (±1.64)	104.3 (±3.73)	107.2 (±1.48)	105.0 (±3.86)

*The length of pore edge per unit surface area ($\times 10^3$ μm^2).

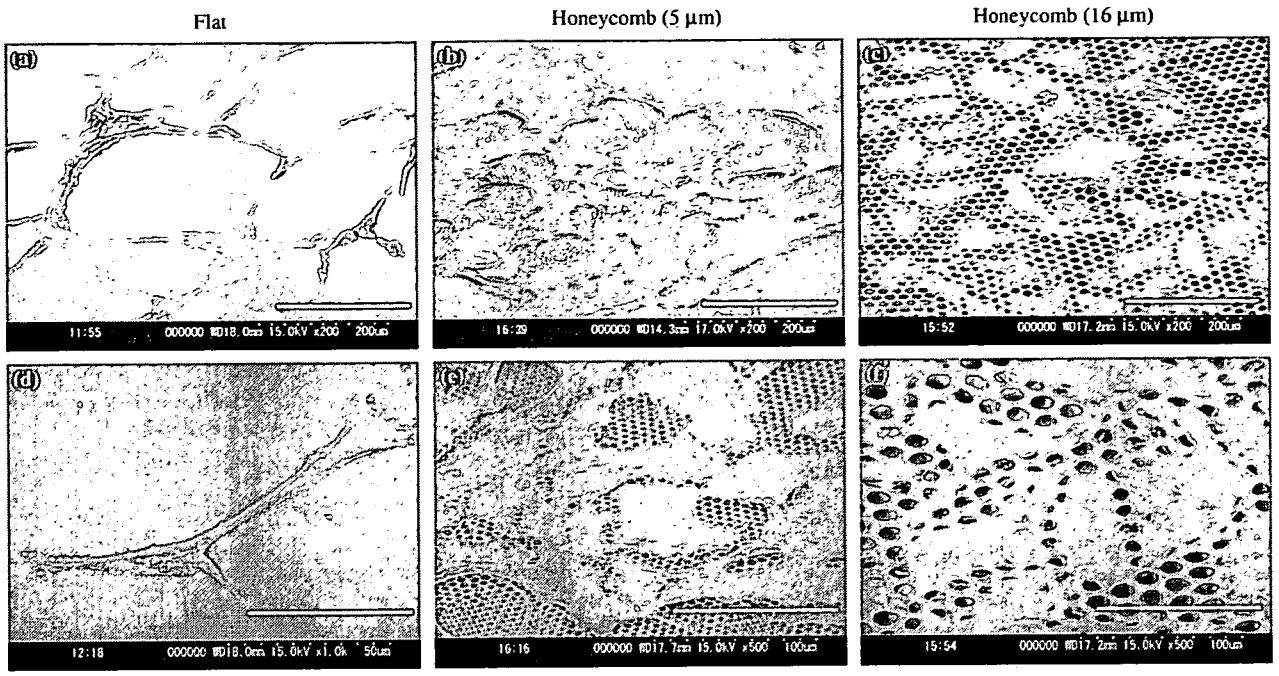

Fig. 4. SEM images of ECs cultured on the flat and honeycomb films. (a), (d): Cultured on the flat film for 5 days. (b), (e): Cultured on the honeycomb film (pore size, approximately 5 μm) for 5 days. (c), (f): Cultured on the honeycomb film (pore size, approximately 16 μm) for 3 days. Bar: (a), (b), (c) 200 μm; (d) 50 μm; (e), (f) 100 μm.

3.3. Proliferation Behavior of ECs on Honeycomb Films with Different Pore Sizes

Cell adhesion is a key step that occurs before cell proliferation. The variation in the cell adhesion may influence the cell proliferation. Figure 5 shows the proliferation profiles of ECs cultured on the honeycomb films. The number of ECs on the honeycomb film was compared with that of those on the flat film. The cell number tended to increase with incubation time, irrespective of the pore size of the honeycomb film. The honeycomb film with a pore size of 5 μm showed the highest proliferation. The number of cells on the honeycomb films was nearly two times that on the flat films. The proliferation increased with time for the initial 5 days and was saturated on day 7. The initial rate of cells grown was higher for the honeycomb films with 24 h culture, but once the cells reached confluent, the proliferation stopped. Figure 6 shows the SEM images of ECs on honeycomb films with different pore sizes. After 7 days of culture, the ECs were well spread and were able to form a confluent monolayer on the honeycomb film with a pore size of 5 μm.

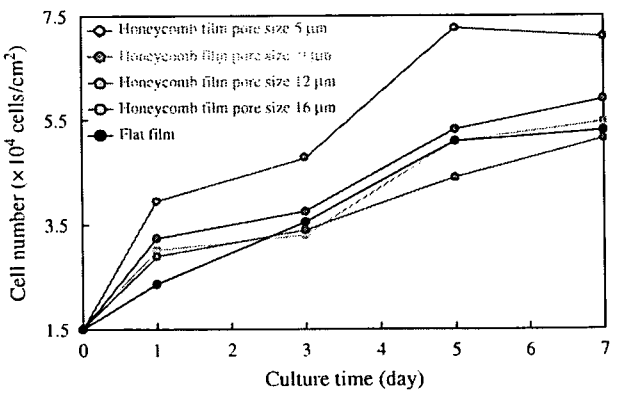

Fig. 5. Proliferation of the cultured ECs on the flat and honeycomb films.

The proliferation of cells on a scaffold requires oxygen and nutrient supply. The scaffold materials should provide such an environment for cells. The results of the cell adhesion and proliferation profiles (Figs. 5 and 6) revealed that diffusion of nutrients, bioactive factors, and oxygen and the exchange of wastes from the cells that was facilitated through these highly interconnected pores was sufficient for the survival of a large number of cells for extended periods of time. The honeycomb film may not only provide mechanical support for cells but also serve as a medium through which diffusion of soluble factors can occur. If the honeycomb film can promote the adhesion and growth of cells on its surface, it could have important biomedical applications.

3.4. Actin Filaments and Focal Adhesions

To clarify the reason for the greater cell proliferation on the 5 μm pore sized honeycomb film compared to the other films, the direct effect of the honeycomb films on the spatial arrangement of the cytoskeleton as well as on focal adhesion was investigated. Cytoskeletal actin is known as a liner protein that determines cell shape. In addition, it is also important in cellular functions and proliferation.

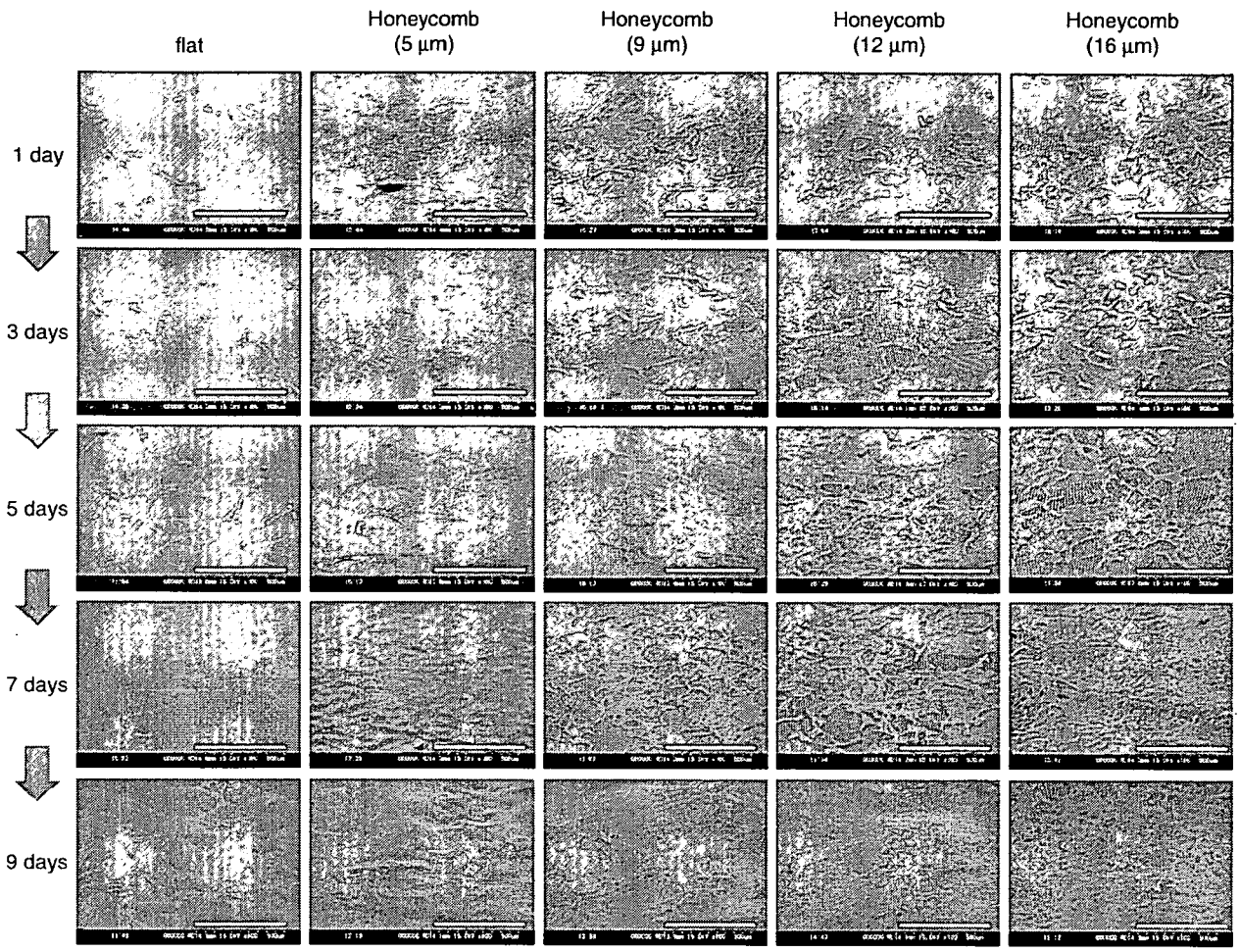

Fig. 6. SEM images of the ECs cultured on the flat and honeycomb films. Bar: 500 μm.

These events involve the development of specific intercellular adhesions and redistribution of cell–cell and cell–material adhesion forces that are intimately related to the dynamic cytoskeletal organization. Figures 7(a–c) shows the CLSM images of the actin filaments in the ECs adhered to both the flat and honeycomb films. The actin filaments were clearly observed in the spreading regions of the ECs on the honeycomb film (Figs. 7(b, c)). However, the actin filaments could not be clearly observed on the flat film (Fig. 7(a)). These results indicated that the honeycomb film could control EC adhesion following cytoskeletal protein production.

The cell proliferation is highly regulated by cell adhesion onto biomaterials. Focal adhesion proteins such as vinculin play a crucial role in cell-adhesion behavior and are major cellular sites responsible for cell–protein attachment. The morphology of focal adhesion was clearly different in the honeycomb film (Figs. 7(h, i)) and the flat film (Fig. 7(g)). The analysis of the confocal microscopy images showed that the focal adhesions could not be formed properly on the flat film (Fig. 7(g)). The focal adhesions existed locally at the intracellular edge of the elongated cells on the flat film. In contrast, the focal adhesions were localized along the edge of the honeycomb pores that were distributed over the entire projected cell area (Figs. 7(h, i)). The distribution of focal contacts along the pore edges suggests that strong adhesion sites were formed on the honeycomb film; however the flat film showed weak focal contacts. The honeycomb film with a pore size of 5 μm showed the highest number of focal adhesions due to a combination of the greater pore numbers and the length of pore edge per unit surface area. This implies that a higher focal adhesion density may induce a complex signal transduction for the proliferation of ECs. The site-selective distribution of focal adhesions indicates that ECs adhere to adsorbed proteins on the honeycomb rims. It was suggested that the difference in the cell proliferation properties of these films is caused by the difference in focal adhesions. In our experiments, the stained focal adhesion sites that existed at the intracellular edge were found to be composed of actin joined together with vinculin (Figs. 7(d–f)).

The results are of interest with regard to the Rho family of small GTPase. The Rho family has emerged as the key regulator of the actin cytoskeleton and it coordinates cellular activities, such as gene transcription and adhesion.[31]

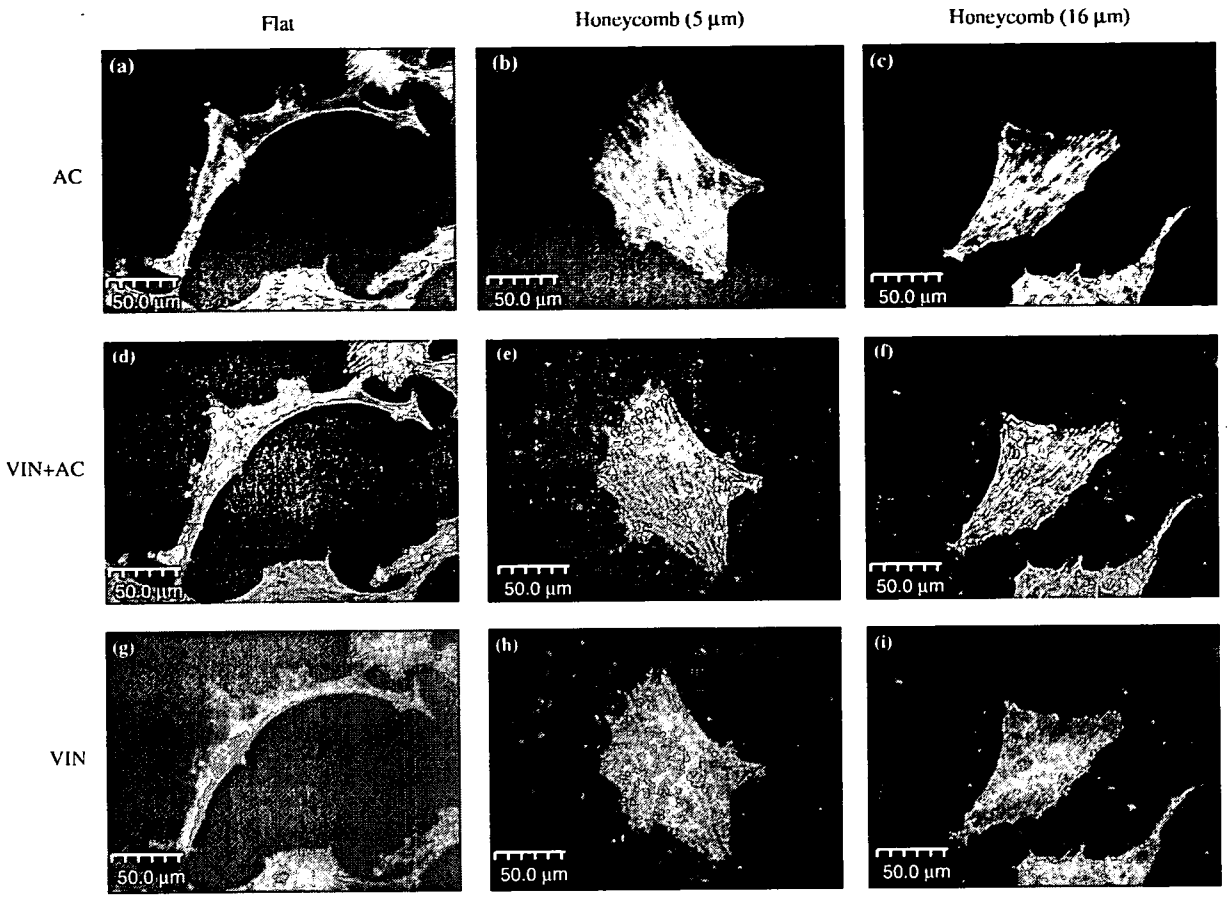

Fig. 7. CLSM images of ECs cultured on flat and honeycomb films. The cytoskeletal protein actin filaments and vinculin are stained using immunofluorescence. (a), (b), (c): Actin filaments. (d), (e), (f): Actin filaments and vinculin. (g), (h), (i): Vinculin. (a), (d), (g): Cultured on the flat film for 3 days. (b), (e), (h): Cultured on the honeycomb film (pore size, approximately 5 μm) for 3 days. (c), (f), (i): Cultured on the honeycomb film (pore size, approximately 16 μm) for 3 days. Bar: 50 μm.

It is possible that the topological properties of the honeycomb film affected the signal transduction involving the Rho family since morphology, actin localization, and focal adhesions of ECs on the honeycomb film were different from those on the flat film.

3.5. ECM Production

The EC morphology, formation of actin filaments, and focal adhesions are important factors that affect the EC function. The secretion of ECM is one of the EC-specific functions; therefore, we investigated the secreted ECM profiles. Figure 8 shows the data on ECM (fibronectin, laminin, type IV collagen, and elastin) production profiles 5 days after culture on both the flat and honeycomb films. The ECM production level in the cultured ECs on the honeycomb film was relatively high compared to that of those on the flat film. Collagen IV formed a dense fibrillar network on the honeycomb films with a pore size of 5 μm. This indicates that the cells exhibited more specific functions compared with those of the cells on the flat film. As mentioned above, the result indicated that ECM production reflected the morphology of the ECs since the relationship between morphology and functions was known. It was believed that the ECs on the honeycomb film tended to form tissue-like structures, and therefore, a high expression of ECM was observed. These results suggest that the honeycomb film may allow the enhancement and maintenance of EC function for a long period of time.

It is only recently that systematic studies involving surface chemistry and topography have received significant attention.[4,25–27,30] To date, topographic features have been shown to incite changes in the morphology of adherent cells. Several hypotheses regarding the mechanism of cellular reaction to topographical features have been proposed based on the geometrical details of the features that the cells may encounter. It is clear that the major cellular components responsible for these observations include actin filaments, focal adhesions, and outside to inside signal transducers such as integrins.[32–37] The topographic features also affect gene expression and protein synthesis and may influence other parts of the cellular machinery. However, the mechanism of the topological effect on cell behavior is still not well understood.

We found that the honeycomb film considerably affected not only cell adhesion but also proliferation and ECM

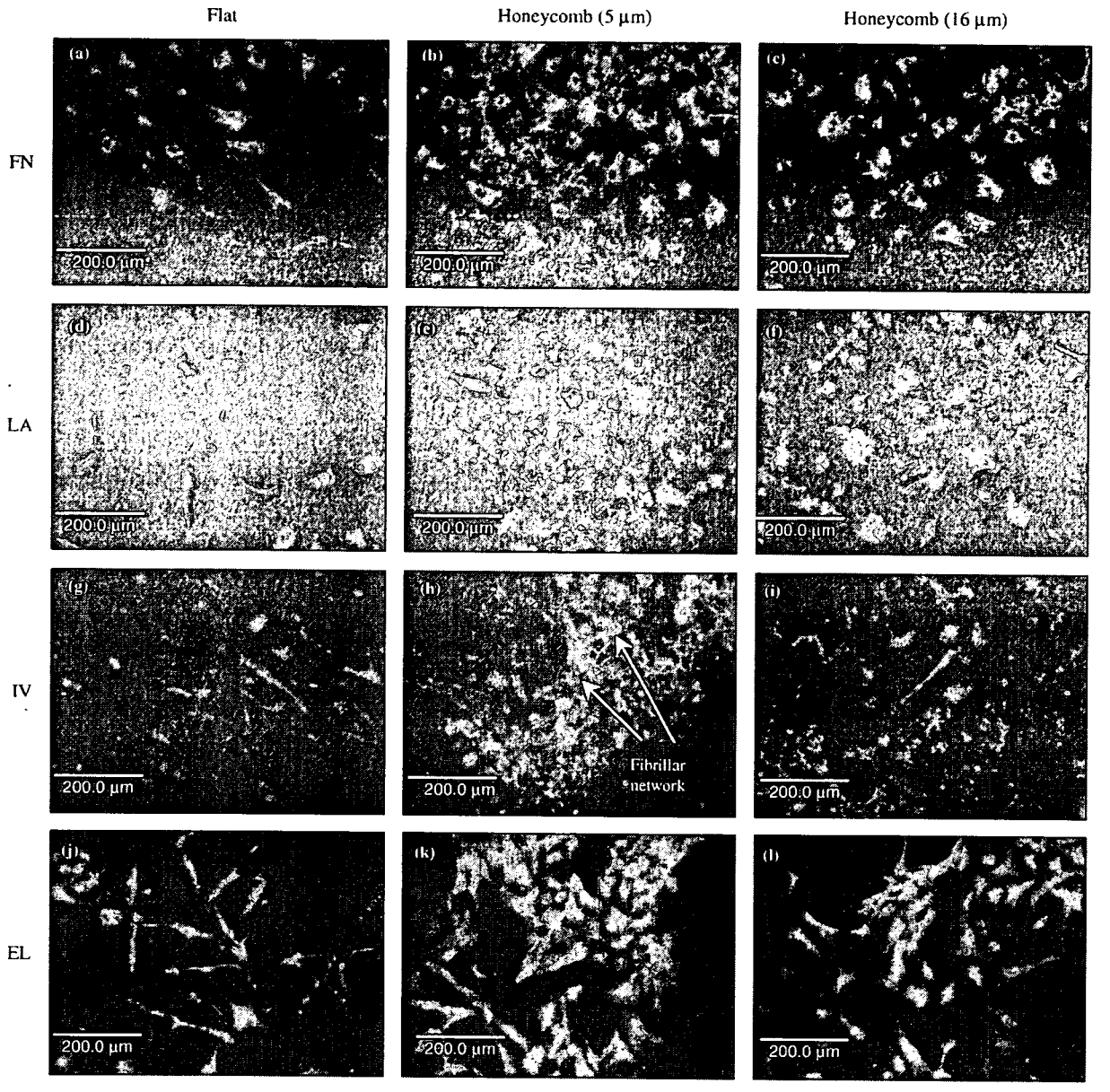

Fig. 8. CLSM images of ECs cultured on the flat and honeycomb films. Fibronectin, laminin, type IV collagen, and elastin are stained using immunofluorescence. (a), (b), (c): Fibronectin. (d), (e), (f): laminin. (g), (h), (i): Type IV collagen. (j), (k), (l): Elastin. Bar: 200 μm.

production of the ECs following actin and vinculin organization. These results indicate that the physical properties of films should be considered in the cases where porous films are used as scaffolds. The relationships between cell adhesion, cytoskeletal elements, focal adhesions, cell functions, and the dimensions of surface pattern are not fully understood. To date, there is little information regarding porous film-induced topological effects on ECs, although an optimal balance between the degree of cell–cell and cell–material interactions has been recognized as a critical factor for guiding three-dimensional cellular organization and improving EC functions on porous films used as tissue engineering scaffolds. The honeycomb film is also a useful tool for obtaining insights into the mechanism of cell–cell and cell–material interactions, which is one of the central research topics in tissue engineering.

At present, the mechanism by which the cells recognize the honeycomb film in cultures is unclear. It is generally known that the adhesion and morphology of cells are influenced by the variety and structure of proteins adsorbed on the material surface.[38] We have reported the adsorbed proteins and water on polymers in order to clarify the main factor that causes cell–material and protein–material interactions.[39,40] We have also reported that fibronectin that is site-selectively adsorbed onto the honeycomb film plays vital roles in cell adhesion, focal adhesion, and proliferation. It was demonstrated that the honeycomb film influenced cell behavior via the site-selectively adsorbed fibronectin molecules.[41,42] This type

of study will continue to play a key role in the characterization of the surface of honeycomb films that affect cell adhesion. Other interface characterization techniques using spectroscopy, microscopy, and diffraction would provide additional information and extend our understanding of the role of honeycomb film surfaces. Since the mechanisms involved in the cellular response to topography are quite complex, further research is required to elucidate the influence of a honeycomb-patterned surface on the biochemical pathways and cellular signaling mechanism that regulate cell adhesion and functions. This complete understanding of cell–material surface interactions will pave the way for successful implantation of biomaterials.

4. CONCLUSIONS

ECs were cultured on the honeycomb films in order to investigate the influence of the honeycomb pattern and the pore size on cell behavior. Honeycomb films exert a strong influence on cell morphology, proliferation, cytoskeleton, focal adhesion, and ECM production profiles. Our studies demonstrated that the cellular behaviors are controlled by the pore size of the honeycomb film. ECs showed increased spreading and flattening on the honeycomb film and expressed proper EC-specific functions. The focal adhesions existed locally along the intracellular edge of the elongated cells on the flat film. However, on the honeycomb film, the focal adhesions were localized along the edge of the pores distributed over the entire projected cell area. The honeycomb film with a pore size of 5 μm showed the highest number of focal adhesions. This implies that a higher focal adhesion density may induce a complex signal transduction for EC proliferation and functions. Fabrication of honeycomb films by self-organization would be an effective method that does not require lithography or consume a large amount of energy. The technology for fabricating 3-D honeycomb films with well-controlled pore sizes may be useful for constructing porous films with controlled pore sizes to improve cell performance. *In vivo* application of honeycomb films as a small diameter tubular scaffold is currently under evaluation; it may be an effective strategy for vascular tissue engineering.[43]

Acknowledgments: This work is supported by Grants-in-Aid and CREST from Japan Science and Technology Corporation (JST) and Special Coordination Funds for Promoting Science and Technology of Ministry of Education, Culture, Sports, Science and Technology.

References and Notes

1. L. G. Cima, J. P. Vacanti, and C. Vacanti, *J. Biomech. Eng.* 113, 143 (1991).
2. L. G. Griffith, B. Wu, and M. J. Cima, *Ann. N.Y. Acad. Sci.* 831, 382 (1997).
3. A. G. Mikos, Y. Bao, and L. G. Cima, *J. Biomed. Mater. Res.* 27, 183 (1993).
4. C. S. Chen, M. Mrksich, S. Huang, G. M. Whitesides, and D. E. Ingber, *Science* 276, 1425 (1997).
5. P. Clark, S. Britland, and P. Connolly. *J. Cell Sci.* 105, 203 (1993).
6. M. C. Wake, P. K. Gupta, and A. G. Mikos. *Cell Transplantation* 5, 465 (1996).
7. L. D. Harris, B. S. Kim, and D. J. Mooney, *J. Biomed. Mater. Res.* 42, 396 (1998).
8. L. Kam, W. Shain, J. N. Turner, and R. Bizios, *Biomaterials* 22, 1049 (2001).
9. J. Tan and W. M. Saltzman, *Biomaterials* 23, 3215 (2002).
10. J. B. Recknor, J. C. Recknor, D. S. Sakaguchi, and S. K. Mallapragada, *Biomaterials* 25, 2753 (2004).
11. S. J. Hollister, *Nat. Mater.* 4, 518 (2005).
12. N. Maruyama, T. Koito, J. Nishida, T. Sawadaishi, X. Cieren, K. Ijiro, O. Karthaus, and M. Shimomura, *Thin Solid Films* 327/329, 854 (1998).
13. O. Karthaus, N. Maruyama, X. Cieren, M. Shimomura, H. Hasegawa, and T. Hashimoto, *Langmuir* 16, 6071 (2000).
14. M. Shimomura and T. Sawadaishi, *Curr. Opin. Colloid Interf. Sci.* 6, 11 (2001).
15. K. Sato, M. Tanaka, K. Hasebe, M. Takebayashi, K. Nishikawa, T. Kawai, M. Matsushita, S. Todo, and M. Shimomura, *Int. J. Nanosci.* 1, 689 (2002).
16. T. Nishikawa, R. Ookura, J. Nishida, K. Arai, J. Hayashi, N. Kurono, T. Sawadaishi, M. Hara, and M. Shimomura, *Langmuir* 18, 5734 (2002).
17. H. Yabu, M. Tanaka, K. Ijiro, and M. Shimomura, *Langmuir* 19, 6297 (2003).
18. M. Tanaka, M. Takebayashi, M. Miyama, J. Nishida, and M. Shimomura, *Bio-Med. Mater. Eng.* 14, 439 (2004).
19. A. Tsuruma, M. Tanaka, N. Fukushima, and M. Shimomura, *e-J. Surf. Sci. Nanotechnol.* 3, 159 (2005).
20. H. Yabu, M. Takebayashi, M. Tanaka, and M. Shimomura, *Langmuir* 21, 3235 (2005).
21. J. Nemoto, Y. Uraki, T. Kishimoto, Y. Sano, R. Funada, N. Obata, H. Yabu, M. Tanaka, and M. Shimomura, *Bioresource Technol.* 96, 1955 (2005).
22. Y. Fukuhira, E. Kitazono, T. Hayashi, H. Kaneko, M. Tanaka, M. Shimomura, and Y. Sumi, *Biomaterials* 27, 1797 (2006).
23. M. Tanaka, K. Nishikawa, H. Okubo, H. Kamachi, T. Kawai, M. Matsushita, S. Todo, and M. Shimomura, *Colloids Surf. A* 284–285, 464 (2006).
24. A. Tsuruma, M. Tanaka, S. Yamamoto, N. Fukushima, and M. Shimomura, *Colloids Surf. A* 284–285, 470 (2006).
25. A. Curtis and C. Wilkinson, *Biomaterials* 18, 1573 (1997).
26. X. Jiang, S. Takayama, X. Qian, E. Ostuni, H. Wu, N. Bowden, P. LeDuc, D. Ingber, and G. M. Whitesides, *Langmuir* 18, 3273 (2002).
27. H. S. Nalwa (ed.), Handbook of Nanostructured Biomaterials and Their Applications in Nanobiotechnology, American Scientific Publishers, Los Angeles (2005), Vols. 1–2.
28. M. S. Baguneid, A. M. Seiflian, H. J. Salacinski, D. Murray, G. Hamilton, and M. G. Walker, *Br. J. Surg.* 93, 282 (2006).
29. S. Nishimura and K. Yamada, *J. Am. Chem. Soc.* 119, 10555 (1997).
30. P. Uttayarat, G. K. Toworfe, F. Dietrich, P. I. Lelkes, and R. J. Composto, *J. Biomed. Mater. Res.* 75, 668 (2005).
31. A. Hall, *Science* 279, 509 (1998).
32. D. E. Ingber, *Proc. Natl. Acad. Sci. USA* 87, 3579 (1990).
33. R. Singhvi, A. Kumar, G. P. Lopez, G. N. Stephanopoulos, D. I. C. Wang, G. M. Whitesides, and D. E. Ingber, *Science* 264, 696 (1994).
34. A. J. Garcia, M. D. Vega, and D. Boettiger, *Mol. Biol. Cell.* 10, 785 (1999).

35. N. Pernodet, M. Rafailovich, J. Sokolov, D. Xu, N. L. Yang, K. McLeod, *J. Biomed. Mater. Res.* 64, 648 **(2003)**.
36. M. Arnold, A. Cavalcanti-Adam, R. Glass, J. Blümmel, W. Eck, M. Kantlehner, H. Kessler, and J. P. Spatz, *Chem. Phys. Chem.* 5, 383 **(2004)**.
37. N. D. Gallant, K. E. Michael, and A. J. García, *Mol. Biol. Cell* 16, 4329 **(2005)**.
38. J. D. Andrade (ed.), Surface and Interfacial Aspects of Biomedical Polymers, Plenum Publishers, New York **(1985)**, p. 1.
39. M. Tanaka, A. Mochizuki, N. Ishii, T. Motomura, and T. Hatakeyama, *Biomacromolecules* 3, 36 **(2002)**.
40. M. Tanaka and A. Mochizuki, *J. Biomed. Mater. Res.* 68A, 684 **(2004)**.
41. S. Yamamoto, M. Tanaka, H. Sunami, S. Yamashita, Y. Morita, and M. Shimomura, *Surf. Sci.* 600, 3785 **(2006)**.
42. H. Sunami, E. Ito, M. Tanaka, S. Yamamoto, and M. Shimomura, *Colloids Surf A* 284–285, 548 **(2006)**.
43. M. Tanaka, Patent pending (JP2005-281268).

Received: 12 March 2006. Accepted: 22 May 2006.

TISSUE ENGINEERING
Volume 13, Number 4, 2007

DOI: 10.1089/ten.2006.0321

Small-Diameter Porous Poly (ε-Caprolactone) Films Enhance Adhesion and Growth of Human Cultured Epidermal Keratinocyte and Dermal Fibroblast Cells

JAMES R. MCMILLAN, M.Sc., Ph.D.,[1,2] MASASHI AKIYAMA, M.D., Ph.D.,[1] MASARU TANAKA, Ph.D.,[2] SADAKI YAMAMOTO, Ph.D.,[2] MAKI GOTO, Ph.D.,[1] RIICHIRO ABE, M.D., Ph.D.,[1] DAISUKE SAWAMURA, M.D., Ph.D.,[1] MASATSUGU SHIMOMURA, Ph.D.,[2] and HIROSHI SHIMIZU, M.D., Ph.D.[1]

ABSTRACT

Autologous keratinocyte grafts provide clinical benefit by rapidly covering wounded areas, but they are fragile. We therefore developed biocompatible hexagonal-packed porous films with uniform, circular pore sizes to support human keratinocytes and fibroblasts. Cells were cultured on these porous poly (ε-calprolactone) films with pore sizes ranging from novel ultra-small 3 μm to 20 μm. These were compared with flat (pore-less) films. Cell growth rates, adhesion, migration, and ultrastructural morphology were examined. Human keratinocytes and fibroblasts attached to all films. Furthermore, small-pore (3-5 μm) films showed the highest levels of cell adhesion and survival and prevented migration into the pores and opposing film surface. Keratinocyte migration over small-pore film surface was inhibited. Keratinocytes optimally attached to 3-μm-pore films due to a combination of greater pore numbers (porosity), a greater circumference of the pore edge per unit surface area, and greater frequency of flat surface areas for attachment, allowing better cell–substrate and cell–cell attachment and growth. The 3-μm pore size allowed cell–cell communication, together with diffusion of soluble nutrients and factors from the culture medium or wound substrate. These characteristics are considered important in developing grafts for use in the treatment of human skin wounds.

INTRODUCTION

THERE HAVE BEEN NUMEROUS REPORTS OF micro-scale and nano-scale structured materials with biologically significant properties using basic chemical composition and micro- or nano-scale structural features that may influence cell characteristics grown on these materials.[1–5] Studies examining this phenomenon include those exploring fibrovascular connective tissue cultured on foams,[6,7] osteoblasts grown on porous surfaces,[8,9] tissue fibroblasts on porous membranes,[10] and mouse 3T3 fibroblast-maintained porous collagen–glycosaminoglycan scaffolds.[11] The typical cell responses to nano- and micro-scale structure and geometry include changes in cell adhesion, proliferation, and survival on smaller-scale structures and altered morphology, including cell size, shape, and orientation.[6,7,12,13] Material pore size has emerged as a significant factor affecting cell adhesion and growth on culture substrates; however, the pore shape in many experimental biomaterials has been irregular and had poor uniformity of pore distribution, with variable, generally poorly controlled pore size.[7,10,14,15] We have developed a low-cost process of porous film manufacturing using biocompatible poly (ε-caprolactone) (PCL) material that produces a regular, controlled pore size and a regular, hexagonally packed pore distribution on a flat film.[16–19]

[1]Department of Dermatology, Hokkaido University, Graduate School of Medicine, Sapporo, Japan.
[2]Creative Research Initiative Sousei, Faculty of Science, Hokkaido University, Sapporo, Japan.

Unsupported human skin grafts in current use are composed of keratinocyte sheets and are thin, fragile grafts that must be removed from a donor site, causing further patient injury, and later applied to pre-prepared, cleaned wounded areas to aid rapid wound coverage and achieve effective results. Additional support of these cultured autologous grafts, especially during the handling process, is desirable to improve graft application. Aliphatic polymers such as those made from PCL provide sufficient strength, support, and flexibility and are also biocompatible and biodegradable in the human body. (They are already being used in surgical sutures and blood vessel stents or supports.[13,20]) The porous film also provides an occlusive surface to separate distinct groups of cells on opposite sides; the size of the film pores can precisely control the wound bed connective tissue cells and cultured epithelial cells and the extent to which these two cells types interact.[21] In addition, the center of the pore can itself be used to store or protect biological structures, for example, adhesion components or growth factors encapsulated in controlled-release technologies. Previously, the range of pore sizes that have been regularly and uniformly fabricated has been between 5 and 20 μm in diameter because of limitations in the polymer and solvent used.[19,22,23] Here, we demonstrate that this limit has been extended to grow skin-derived cells on the smallest pores (3 μm) that can be fabricated using self-organizing processes. The precise control of regular pore size limits cell adhesion and communication as well as allowing storage of bioactive compounds provides an important benefit to using the porous films as graft substrates.

We have developed a way to easily and cheaply prepare a regular, patterned surface on which cells can be grown that allow it to be used as a graft to improve wound healing. Our novel porous PCL films (devised and patented by Creative Research Initiative Sousei, Hokkaido University, see patents by Tanaka et al.[1] McMillan et al.[2]) have been tested as a biodegradable platform to support cultures of various human cells.[16,18,24,25] Furthermore, we report here the first fabrication and use of ultra-small-pore-size films with 3-μm-sized pores and report the effects culturing the 2 main skin-derived cells, keratinocytes and fibroblasts, grown on this substrate.

To investigate the effect regular porous films have on monocultures of skin cells, we have investigated the properties of cultured human epidermal keratinocyte and dermal fibroblast cell adhesion, migration, growth, and morphology on different-sized pore substrates. The aim of this study is to enhance our understanding of the processes of cell–substrate interactions and how these factors affect cell adhesion, growth, migration, and morphology. This knowledge will allow us to make further improvements to optimize skin graft efficacy and improve wound healing.

[1]Biodegradable honeycomb films for tissue engineering scaffolds (Patent number: 1999-340568(JP). Application date: 1999/11/30.) Biomedical devices (Patent number: 2001-342484 (JP). Application date: 2001/11/07.)

[2]Porous honeycomb films: applications for cultured human keratinocyte and fibroblast composite grafts and human skin equivalents (Patent number: 2005-188948(JP). Application date: 2005/06/28.)

MATERIALS AND METHODS

Preparation of porous films

The porous PCL uniform 3-dimensional porous films were manufactured using previously described procedures.[16,26,27] Films were disinfected and sterilized (using ethanol and ultraviolet light sterilization), washed, an dair dried, and trapped air was removed using a combination of serial ethanol and sterile 0.1 M Dulbecco's phosphate buffered saline (PBS) washes (Invitrogen/Gibco, BRL, Carlsbad, CA). The sterilized porous films were then directly seeded with monocultures of keratinocytes or fibroblasts. The production procedure uses polymer–solvent mixtures to form perfectly spherical solvent-filled spaces, and thereby pores, in the films. Thus, pore size and depth are intrinsically linked.

Cell sources

The cells (keratinocytes and fibroblasts) were seeded on the upper surface of the film only. Fibroblast cells were sustained in Dulbecco's modified Eagle medium (DMEM) with 10% fetal calf serum, penicillin, and streptomycin (Cambrex, Walkersville, MD) for 24 h to 10 days. Keratinocytes were cultured in keratinocyte growth medium (KGM) I (Cambrex, Walkersville, MD) for between 24 h and 10 days. Normal human neonatal foreskin keratinocytes (Cambrex) were grown in KGM I culture medium (Clonetics, Walkersville, MD) until passage 2 or 3 (P2/P3). The cells were then trypsinized and stored in 10% dimethyl sulfoxide (DMSO) under liquid nitrogen until needed. Normal human dermal fibroblasts were obtained (Cambrex) and grown in DMEM (Cambrex) until P2. Cells were then trypsinized and stored in 10% DMSO under liquid nitrogen until required.

Cell adhesion and growth assays

Normal human neonatal keratinocytes (P2/P3) or dermal fibroblasts (P2) were grown in appropriate culture medium. Cells were trypsinized and counted and 3×10^5 cells plated onto 16-mm-diameter sterilized circular glass-supported substrates including flat (pore-less) PCL film and porous PCL films. This density has previously been determined to be more than sufficient for proper seeding of keratinocyte grafts.[28] Cells were left to adhere for 2 or 24 h to these films with various sized pores. After this time period, the plates were washed 4 times in sterile 0.1 M Dulbecco's PBS and the numbers of live keratinocytes counted after a 5-min incubation with 0.05 μg/mL of acetoxymethyl ester (AME,

C-369), a fluorescent marker for live cells (Molecular Probes, Eugene, OR), in PBS followed by two 5-min washes each in PBS and then DMEM. Only live cells (keratinocytes or fibroblasts) are able to deacetylate the non-fluorescent protein, converting it into fluorescent form. Attached cells were immediately counted using an Olympus Fluoview FV300 confocal and IX70 inverted microscope (Olympus, Tokyo, Japan). Only attached, live, uniformly fluorescent cells were counted on each substrate at a single time point (24 h after initial plating). The mean number of live cells per high power field ($n > 10$) per substrate was calculated. This experiment was repeated 3 times. The treatment groups were compared using one-way analysis of variance (ANOVA) and two sample t-tests using the Minitab statistical package (Minitab Inc., University of Pennsylvania, Philadelphia, PA) at $p < 0.05$ or <0.01 showing significant effects.

For the cell-growth assay, P2-P3 cells were grown on flat or porous films, as previously described,[24] and grown in appropriate culture medium. At specific time points (24, 48, and $\geq$144 h) the plates were washed 4 times in sterile 0.1 M Dulbecco's PBS and the numbers of live cells counted as previously described one directly from phase-contrast photomicrographs. Attached cells were counted using an Olympus IX70 inverted Fluoview FV300 confocal microscope. The numbers of live cells per high-power field ($n > 10$) were calculated per substrate group. Statistical analysis was performed between the treatment groups using one-way ANOVA and two sample t-tests using the Minitab statistical package. The results are shown in Figure 1B and D. This experiment was repeated 3 times.

Migration assay

Normal control P3 keratinocytes or fibroblasts were plated onto substrates (flat calprolactone or porous films). Cells were grown on various substrates in KGM I (keratinocytes) or DMEM (fibroblasts, Clonetics). Cells were grown at between 1×10^5 and 3×10^5 cells per 16-mm well on various substrates as previously described and placed in a temperature- and carbon dioxide (CO_2)-controlled microscopic stage while

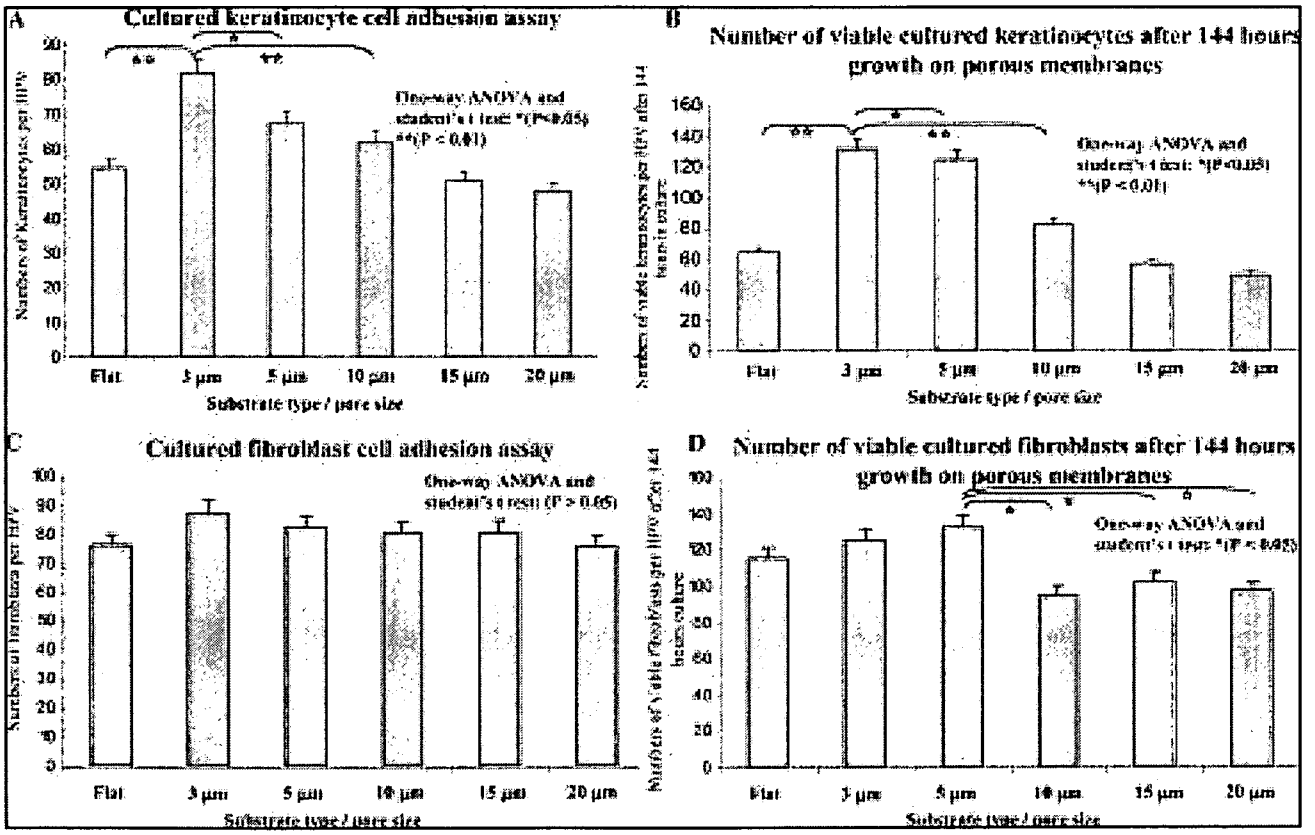

FIG. 1. Keratinocytes show greater increases in cell-substrate adhesion and growth than fibroblasts on porous poly(ε-caprolactone) films. Keratinocyte adhesion assays over 24 h **(A)** demonstrated statistically significantly ($p < 0.01$) greater keratinocyte adhesion between 3 μm porous films than between all other larger films. **(B)** Keratinocyte growth assay over 144 h (6 days) showed a similar ranking but also more-significant differences between 3-μm and other films. Fibroblast adhesion rates over 24 h showed no significant changes when these cells were plated on different films **(C)**. **(D)** The fibroblast growth rate over 144 h showed moderate differences ($p < 0.05$) between the flat, 3-μm, and 5-μm group and the larger-pore 10-μm, 15-μm, and 20-μm group. For fibroblasts, the 5-μm films appeared optimal for growth. Statistical analysis: one-way analysis of variance (ANOVA) and Student t tests. *ANOVA, $p < 0.05$, **$p < 0.01$). Error bars 1 = standard deviation.

cells were observed using video microscopy using an INU-NI series microscope stage fitted to an inverted TE 2000 microscope (Nikon, Tokyo, Japan). Single-cell migration assays using time-lapse digital video microscopy were performed for periods of between 8 and 24 h. The number of cells observed using video microscopy was greater than 50 cells per group. Cells were observed using a time-lapse video interval of 5 min, and the distance traveled was observed using a precalibrated scale and MCID/M2 image analysis software (Imaging Research Inc., Ontario, Canada). Cell viability counts were confirmed after 5 min incubation with 0.05 μg/mL of C-369 AME, a fluorescent marker for live cells (Molecular Probes), and examination under a confocal microscope as previously described. The average distance traveled per hour was calculated for each cell type on each substrate. Statistical analysis was performed to compare the treatment groups using one-way ANOVA and two sample t-tests using the Minitab statistical package.

Scanning electron microscopy

Cells grown on various substrates for 48 h were fixed in 2% glutaraldehyde for at least 4 h and processed for routine scanning electron microscopy (SEM). Briefly, samples were dehydrated in a graded ethanol series, treated twice with isoamyl acetate, and critical point CO_2 dried using a Hitachi HCP-2 followed by platinum-palladium sputter coating in a Hitachi E-1030 (Tokyo, Japan). Specimens were examined using a Hitachi S-4500 scanning electron microscope fitted with a digital image capture system. Approximately 200 adherent cells were examined per group.

Transmission electron microscopy

Cells grown on films for 48 h were fixed in 2% glutaraldehyde solution, post-fixed in 1% osmium oxide, dehydrated, and processed for conventional electron microscopic observation according to the methods described previously.[29] Alternatively, samples were dehydrated using a graded ethanol series but were not treated with propylene oxide. Instead they were washed in 100% ethanol and a methanol–acetic acid mixture and subsequently embedded in white acrylic resin (London Resin Company, Reading, UK) or Lowicryl K11M (Ladd Research Industries, Burlington, VT) to avoid harmful film–solvent interactions that were polymerized using ultraviolet light at 4°C for 48 h. Semithin sections were cut and stained with Richardson's stain.[30] Samples were cut, stained with uranyl acetate and lead citrate, and viewed under a Hitachi H-7100 transmission electron microscope at 75 kV.

Confocal immunofluorescence microscopy

Indirect immunofluorescence was performed as previously described[29] using 3-μm porous films with keratinocyte and 5-μm porous films and fibroblast monocultures in addition to cryostat normal skin sections. The mouse monoclonals M3F7 and LH7:2, recognizing collagen IV and collagen VII, respectively, were used at neat and 1 in 2 dilutions.[29] M3F7 were obtained from the Developmental Studies Hybridoma bank, University of Iowa. A laminin 5 antibody, GB3, directed against the laminin 5 α2 chain (Harlan Sera Laboratory, Loughborough, UK), mouse immunoglobulin (Ig)G vinculin VIN-11-05 (Sigma, St Louis, MI) 1 in 100 dilution, desmoplakin (11F5) used at 1 in 50 dilution, and E cadherin HECD1 were used. 4C7 monoclonal antibody recognizing the laminin 10 was used diluted 1 in 25.[29] The following primary antibodies and sera were also used in this study: anti-human keratin 14, clone LL001 diluted 1 in 2 (gifts from B. Lane, Dundee, UK), anti-talin, TD77 mouse antibody diluted 1 in 200, mouse anti-collagen I (1 in 100), and rabbit polyclonal vimentin diluted 1 in 200 (Abcam, Cambridge, UK) against synthetic talin (amino acids 2269-2541) encoding the polypeptide f actin binding region. Staining for actin was performed using phalloidin and rabbit anti-human actin rabbit IgG antisera (Biomedical Technologies, Stoughton, MS).

Cell and film cryostat sections were fixed in acetone methanol and incubated with primary antibodies and antisera. Sections were incubated with secondary antibodies conjugated to fluorescein isothiocyanate (FITC; rabbit anti-mouse IgG or goat anti-rabbit IgG; 1:200; Dako, Tokyo, Japan). Sections were then labeled with a Topro 3 nuclear counterstain (Jackson Immuno-Research, West Grove, PA, diluted 1 in 20,000). The sections were examined using an Olympus Fluoview FV300 confocal microscope. Controls included normal skin cryostat sections, with PBS substituted for the primary antibody, myeloma supernatant, or an irrelevant immunoglobulin isotype as a negative control. All experiments were performed at least twice.

RESULTS

Cell adhesion and growth assays

Cell adhesion on porous films. Keratinocytes (Fig. 1A) and fibroblasts (Fig. 1C) were able to attach to, adhere to, and grow on all porous films. The initial adhesion of keratinocytes (over 24 h) was greater on the small-diameter porous films (with 3 μm producing the best results, closely followed by the 5-μm, 10-μm, 15-μm, and 20-μm porous films, see Fig. 1A). Keratinocyte adhesion was greatest using the smaller-diameter porous film pores (with 3 μm producing the best results, followed closely by the 5-μm film, Fig. 1). However, overall, cell adhesion to the porous films was significantly greater in human dermal–derived fibroblasts than in human epidermal keratinocytes (Fig. 1A vs 1C). Fibroblasts, overall, showed far less-significant differences (Fig. 1C, $p > 0.05$) between adhesion rates on different films, with only a slight increase in adhesion 3 μm compared to sequential minimal decreases in 5 μm, 10 μm and flat surfaces. These data are in broad agreement with our previous

report that demonstrated high levels of adhesion to various porous films shown by the mouse NIH 3T3 fibroblast cell line.[24]

Cell growth rates. Cell growth rates were assessed for up to 6 days. All culture samples were seeded with the same number of cells on each substrate in each well. After 6 days of culture, live cells were stained and cells counted per randomly selected high-power field. Keratinocytes showed the highest proliferation and/or survival rates on 3-μm porous films, although the 5-μm porous films also demonstrated a slightly slower growth rate. These two samples' growth rates were significantly higher than those of any of the larger-pore films (10 μm > 15 μm > 20 μm) or flat substrate.

Fibroblasts showed similar, high growth levels on the 5-μm and 3-μm pore films and flat substrates. However, they also showed significantly lower growth rates on the larger-pore films (10-μm, 15-μm, and 20-μm pores) than on those with smaller pores. This was an approximately 25% to 30% lower growth rates on films with 10-μm pores than on those with 5-μm pores.

Cell migration over the film surface

Lateral cell migration over the surface of the porous film was analyzed using time-lapse video and image analysis and showed that keratinocyte migration rates were lower after plating of cells onto any PCL film than for keratinocytes grown on plastic[31] (Fig. 2, grey bar flat (poreless) PCL vs porous PCL films). Fibroblast migration was significantly less ($p < 0.05$ and $p < 0.01$) but not completely inhibited after plating on porous films, causing reductions of up to 30% (Fig. 2 white bars flat PCL vs 3-μm and 5-μm PCL film, respectively). The differences here reflect severely slower keratinocyte migration rates on any PCL film than the reported migration of keratinocytes on plastic[31] and gradually slower migration rates of fibroblasts grown on 3-μm and 5-μm films (respectively) than for those grown on pore-less flat films.

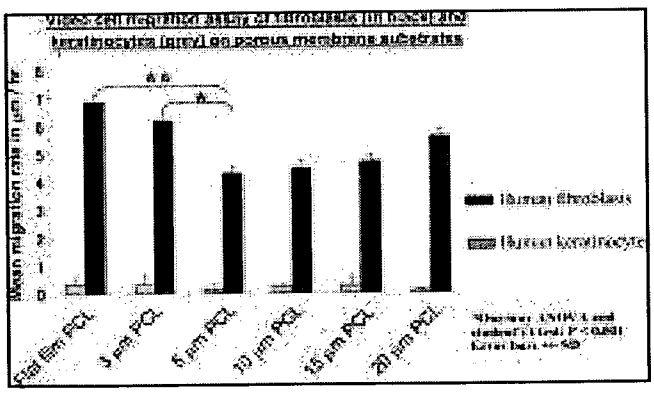

FIG. 2. Video microscopy–assessed migration showed higher migration rates for fibroblasts than for keratinocytes when maintained on porous films. Keratinocyte migration was inhibited on porous membranes, whereas fibroblasts showed the highest migration rates on flat pore-less films, only moderate reductions in migration on 3-μm films and more significant reductions on 5- to 10-μm films. Surprisingly fibroblast migration showed a modest increase on the 20–μm films. Statistical analysis: one-way analysis of variance and Student t tests. $*p < 0.05$, $**p < 0.01$). Error bars 1 = SD.

Migrating cells can cross films with smaller pore sizes more easily than they can cross films with large pores. In addition, the length of pore edge per specific unit surface area is greatest in the small-pore film, which enables cells to use plasma membrane lamleopodia extensions (presumably containing focal contacts) to gain better adhesion on the underlying surface and allow better signal transduction that enable still better adhesion and growth.

Scanning electron microscopy

Keratinocytes seeded onto flat pore-less surfaces attached quickly, spread, and flattened within 2 to 4 h of plating (and were examined using phase contrast microscopy). Cells attached to the underlying substrate using thin filopodial extensions of the plasma membrane that resembled focal adhesions (Fig. 3A–D, white arrows). Keratinocytes subsequently formed small colonies of cells that grew and migrated over the flat films. Keratinocytes on all sizes of porous substrates (Fig. 3B–D) took longer than 48 h to spread (Fig. 3B). Keratinocytes seeded near adjacent cells or those that produced daughter cells after mitotic division maintained desmosome connections (white arrowheads in Fig. 3C) between adjacent cells. Cells were typically positioned over adjacent pores (see Fig. 3B, C). Ultimately, keratinocytes plated on films with pores of any size spread and flattened, covering the film surface with a diameter of as much as 30 to 40 μm (Fig. 3D). Eventually, keratinocytes characteristically formed thin, flat, "fried egg" shapes that covered the pores and surface of the film in equal proportion (Fig. 3D). On the largest-pore films (15–20 μm) occasional individual keratinocytes could be seen within the pores of the film (data not shown).

Fibroblasts grown on flat films quickly attached, spread, and flattened within 3 h (Fig. 3E). Fibroblasts on porous films spread more slowly than on flat films and initially maintained an elongated shape but without significant flattening (Fig. 3F vs E). Eventually, fibroblasts spread and formed flattened shapes covering the porous films as the number of cells increased (Fig. 3G). In larger-pore films (≥5 μm), entire cells were observed that had entered pores, and the cell body passed into the pore space between the upper and lower layers of the film (Fig. 3H, inset). Fibroblasts, because of their thinner, more-elongated shape, were much more frequently observed entering the large film pores (Fig. 3H and inset) than keratinocytes.

Transmission electron microscopic analysis of cells grown on support films

Transmembrane cell migration keratinocytes. Semithin sections showed the basically normal morphology of keratinocytes and fibroblasts grown on flat and porous film supports

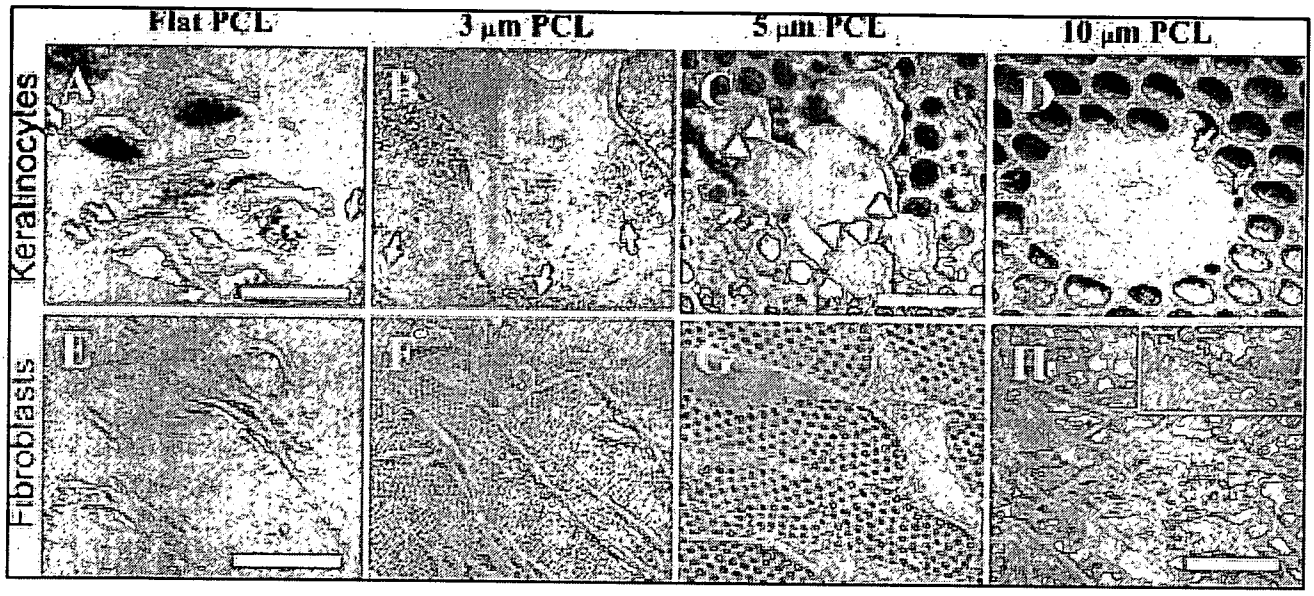

FIG. 3. Scanning electron micrographs showing the morphology of cells grown on flat and porous films after 48 h in culture. Keratinocytes (**A–D**) and fibroblasts (**E–H**) exhibit good cell–substrate attachment on all the surfaces by means of cell projections (filopodia) attaching to the surfaces (arrows in **A**). These cell projections resembled focal adhesion associated lamellipodia/filopodia (arrows in **A–D**). Keratinocytes were slower to spread than fibroblasts but formed flatter, more-rounded cells (**B–D**). Adjacent keratinocytes were able to form close cell–cell associations at possible sites of cell-junction formation (arrowheads in **C**). Conversely, fibroblasts formed small round cells but rapidly (in <1 h) elongated becoming spindle-like cells containing nuclear bulges eventually becoming 25 μm in length. On larger porous films with pores 10 μm and greater, cell processes and entire fibroblasts entered the pores (see inset in **H**). Scale bars (**A, C, E**) 15 μm, (**B, D, F, G, H**) 30 μm.

(Fig. 4A–J). The black dashed lines highlight the upper surface of the flat or porous film (Fig. 4A–J). Keratinocytes seeded on porous films initially showed a rounded morphology and typically sent down small cytoplasmic projections extending 1 to μm into the pores (arrows in Fig. 4C, E, G, I). The number of pores per unit surface area were highest in small-pore (3 μm, Fig. 4C) films and lowest on the large-pore films (15 μm, Fig. 4I; 20 μm, Fig. 4K). (For review of porous film properties, see[22].) This means that keratinocytes grown on small-pore film could form greater numbers of cell projections into the pores per unit surface area than in larger-pore films. In the large-pore films, entire necrotic keratinocytes with pyknotic nuclei were observed within the open pore spaces (Fig. 4K, arrows).

As previously demonstrated using SEM, fibroblasts grown on all porous films showed a flatter morphology than keratinocytes (Fig. 4B). Fibroblasts were also able to extend variable length cell processes and entire cells into the pores, but because these cells were generally longer and thinner than keratinocytes, entire cells were able to enter any pores larger than 5 μm (arrows in Fig. 3F, H, J, L). As the pore size increased beyond 5 μm, increasing numbers of fibroblasts were able to migrate and multiply in the center of the porous films (Fig. 3F, H, J, L).

Transmembrane cell migration. The transmembrane migration of keratinocytes was completely prevented using films with smaller-diameter pored (with the 3- and 5-μm films most effectively preventing transmigration). Only the smallest-pore (3 μm) films were effective at preventing the transmembrane transfer of migrating fibroblasts cells into the spaces in the center of the film. The ratio of pore-size diameter to minimum cell diameter is an important property in determining the extent of cell transmembrane migration into the pores and their subsequent migration to the other side of the porous film. The use of small-pore films might therefore prove advantageous in a graft to avoid the transmembrane transfer of different cell types.

Keratinocyte ultrastructure

Ultrastructure of individual keratinocytes grown on flat and porous films showed a 3- to 4-cell multi-layered but incompletely keratinized epidermis, typical of cells maintained in submerged culture (keratinocytes seeded on 5-μm film Fig. 4M, N). At the apical surface, there were numerous villus-like structures and linking adjacent keratinocytes. There were electron-dense desmosomal plaques associated with keratin intermediate-filament bundles (Fig. 4N, white arrow and inset). At the basal pole of the cultured epidermis, there were severely disorganized keratin filaments, but no basal lamina or well-formed hemidesmosome structures were present (Fig. 4M). Small, hypoplastic hemidesmosomes were occasionally observed along the basal pole but were not attached or associated with any external or underlying structures. Sub-basal dense plates were not observed on

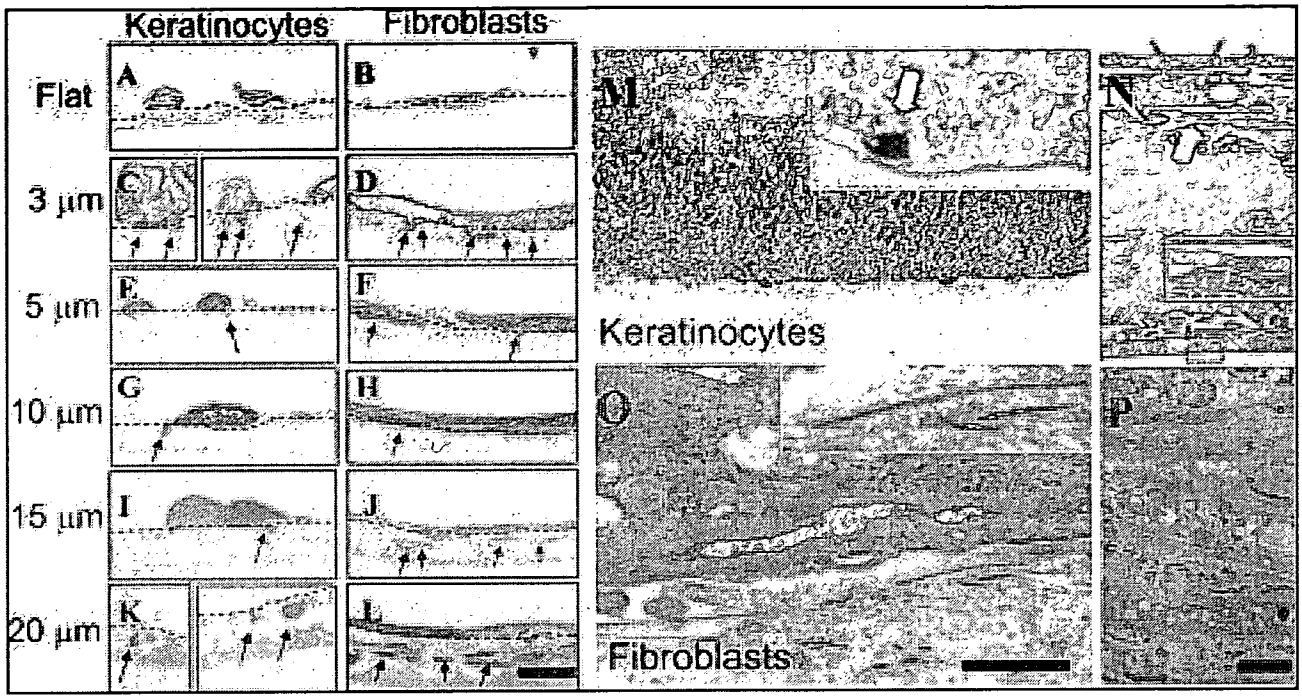

FIG. 4. Semithin and transmission electron microscopy shows the cell morphology, position, and ultrastructure of cells grown on porous films. The dotted lines (**A–J**) highlight the upper surfaces of the films. Both cell types grown on small-pore films (**A–D**, 3-5 μm, arrows) produced filopodial cell projections into the pore space. Furthermore, keratinocytes grown on larger pores (10- to 20-μm-sized pores, **E–J**, arrows) formed larger processes, and on the 20-μm pores, the keratinocytes entered the pore (see arrows in **I**). Often these isolated cells showed pyknotic nuclei and failed to survive (**I**). Fibroblasts were generally longer than even the largest pore size and entered pore sizes greater than 10 μm. The histology of keratinocyte (**H**) and fibroblast (**I**) long-term cultures maintained for 3 weeks shows multiple layers of cells. Ultrastructural analysis of keratinocytes showed no basal lamina or properly formed hemidesmosomes (**M**, arrows, inset in **M**). However, multiple intermediate and microfilaments were observed overlying the keratinocyte plasma membrane (**M, N**). Desmosomes were also seen between keratinocytes (white arrows in **N**, inset). Fibroblasts formed thin, elongated stacks of active cells containing vesicles and mitochondria and collagen fibers between adjacent cells. Scale bar 10 μm (**A–L**), 100 nm (**M, O**), 1 μm (**N, P**). Color images available online at www.liebertpub.com/ten.

any hemidesmosomes. A significant number of substratum-associated actin microfilament bundles were observed at the base of the basal layer keratinocytes (Fig. 4M) and in cell processes (data not shown).

Fibroblast ultrastructure

The ultrastructure of fibroblasts grown on 5-μm porous films showed heterogeneous layers of closely and loosely packed fibroblasts (Fig. 4O, P). Fibroblast morphology was generally that of active cells containing numerous secretory and endocytotic vesicles and together with numerous organelles (Fig. 4P). Cultured fibroblasts typically formed between 2 and 4 cell layers, in which the cells were closely packed or contained intercellular spaces filled with extracellular matrix, ground substance, and cross-banded collagen fibers (Fig. 4O, inset). A significant amount of substratum-associated actin microfilament and (presumably vimentin) intermediate filament bundles were observed within the fibroblasts (Fig. 4O) and in cell processes (data not shown).

Confocal fluorescence microscopy

Keratinocytes cultured on 3-μm films stained with keratin 14 and at the cell borders with the cell adhesion markers desmoplakin and E-cadherin. Keratinocytes showed bright staining for the focal contact and adhesion associated antigens vinculin, actin, and vitronectin but not for the epidermal matrix proteins or the hemidesmosomal anchoring filament protein laminins 5 (332), laminin 10/11 (511 or 521), collagen I, or collagen IV. Collagen VII and fibronectin showed weak epidermal cytoplasmic staining but no evidence of matrix deposition on the film.

Fibroblasts cultured on 5-μm films stained with vimentin (not keratin) and at the cell borders and extracellularly with fibronectin, vitronectin, and collagen I. Fibroblasts showed normal, bright cytoplasmic staining for the focal contact-associated antigens vinculin and actin and weaker staining for talin but no staining for the epidermal matrix proteins laminins 5(332), laminin 10 (511), collagen I, or collagen IV. Collagen VII showed weak cytoplasmic staining with no evidence of matrix deposition on the film.